SUPPLEMENTARY INFORMATION
Study of Ho-doped Bi_2Te_3 topological insulator thin films

S. E. Harrison,[1,2] L. J. Collins-McIntyre,[1] S. L. Zhang,[1] A. A. Baker,[1,3] A. I. Figueroa,[3] A. J. Kellock,[4] A. Pushp,[4] Y. L. Chen,[1] S. S. P. Parkin,[4] J. S. Harris,[2] G. van der Laan,[3] and T. Hesjedal[1,*]

[1] *Department of Physics, Clarendon Laboratory, University of Oxford, Oxford, OX1 3PU, United Kingdom*
[2] *Department of Electrical Engineering, Stanford University, Stanford, California 94305, USA*
[3] *Magnetic Spectroscopy Group, Diamond Light Source, Didcot, OX11 0DE, United Kingdom*
[4] *IBM Almaden Research Center, 650 Harry Road, San Jose, California 95120, USA*

(Dated: October 23, 2015)

I. REFLECTION HIGH ENERGY ELECTRON DIFFRACTION (RHEED)

In-situ reflection high energy electron diffraction (RHEED) was used to provide real-time feedback about the surface morphology of the growing epilayer as a function of the Ho cell temperature. Films were found to exhibit two distinct RHEED patterns along the $[10\bar{1}0]$ and $[11\bar{2}0]$ azimuth of the Al_2O_3 (0001) substrate. These patterns were found to repeat upon 60° rotation, indicative of an $R\bar{3}m$ space group with twinning. As shown in Fig. S1, for Ho cell temperatures up to 865°C, the RHEED patterns observed were well-defined with a streak-like appearance characteristic of a planar surface morphology. At Ho cell temperatures above 865°C, however, the RHEED patterns showed evidence for degradation as the RHEED streaks became more diffuse and developed a spot-like appearance which are indicative of increasing surface disorder and the onset of 3D growth. As a result of these findings, we choose to focus the rest of this study on thin films grown with Ho cell temperatures up to 865°C.

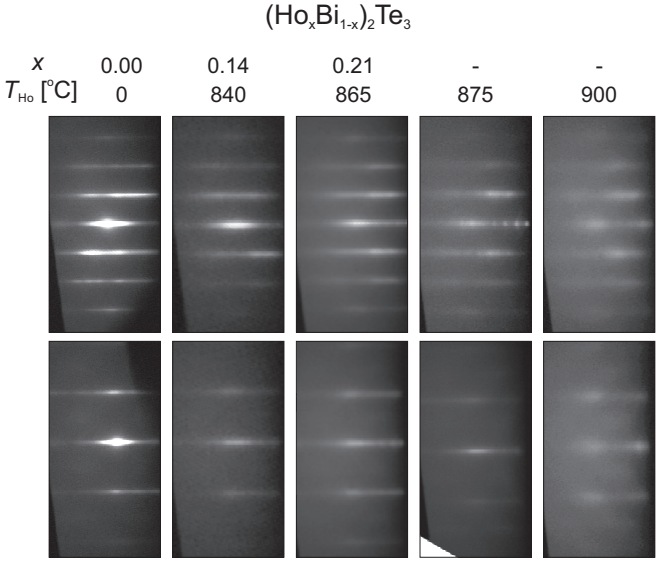

FIG. S1. RHEED patterns of $(Ho_xBi_{1-x})_2Te_3$ films on *c*-plane sapphire for the Ho cell temperatures and concentrations as indicated. Patterns were obtained along the $[10\bar{1}0]$ azimuth (upper row) and along the $[11\bar{2}0]$ azimuth (lower row) of Al_2O_3 (0001). (b,c) SEM images for an $x = 0.14$ film. The scale bar in (b) represents 5 μm and in (c) 500 nm.

II. ROCKING CURVE ANALYSIS

The rocking curves at the (0 0 6) Bragg reflection [e.g., shown in the main text in the inset of Fig. 2(b) for the $x = 0.14$ Ho sample] can be fitted with two Lorentzian functions. One function represents a narrow peak, centered at the maximum of the intensity, and the other function represents a wide background peak, centered at a slightly higher angle. The wider background peak arises from any combination of finite size effects of the domains, tilting at domain boundaries (i.e., mosaicity), as well as interface defects. These broader peaks are systematically offset, indicating some general tilt of the lattice planes with the incorporated dopant.

For comparison, rocking curves at the (0 0 6) reflection for a series of undoped and rare earth doped Bi_2Te_3 thin films, with similar doping concentrations, have been analyzed. A plot comparing the experimental data is shown in Fig. S2. The rocking curves were fitted with two Lorentzian functions and a summary of the fitting parameters are listed in Table II below.

As can be seen in the comparison in Fig. S2, the narrow peak is representative of the undoped and well-ordered portion of the sample. With increasing doping concentration, a relative increase of the broad background peak is observed, which is representative of the doped and more disordered fraction of the sample.[1] Note that the angular separation of the centers of the two peaks is increasing with increasing doping concentration, indicative of a tilt resulting from the dopants.

Among the rare earth series, the FWHMs for the narrow peak were found to vary, with Ho- and Dy-doped films behaving similarly to the undoped Bi_2Te_3. Gd doping, however, shows a much wider peak. For the broader background peak, similar FWHMs were found for all of the films analyzed.

TABLE S1. Rocking curve fits. Two Lorentzian peaks were fitted to the rocking curves at the (0 0 6) Bragg reflection for the dopant, D, as indicated. The doping concentrations in $(D_xBi_{1-x})_2Te_3$ are comparable between $x = 0.11$ and 0.14. Note that the background for the undoped sample is fitted with a Gaussian, representative of the instrument resolution function.

D	x	**Lorentzian 1**		**Lorentzian 2**	
		Peak Center (°)	*FWHM* (°)	*Peak Center* (°)	*FWHM* (°)
undoped	-	8.7136 ± 0.0002	0.0390 ± 0.0001	-	-
Dy	0.11	8.7277 ± 0.0006	0.0352 ± 0.0002	8.7232 ± 0.0005	0.5602 ± 0.0032
Gd	0.12	8.7534 ± 0.0002	0.1013 ± 0.0013	8.7316 ± 0.0007	0.4378 ± 0.0051
Ho	0.14	8.4497 ± 0.0006	0.0456 ± 0.0002	8.4811 ± 0.0003	0.5449 ± 0.0014

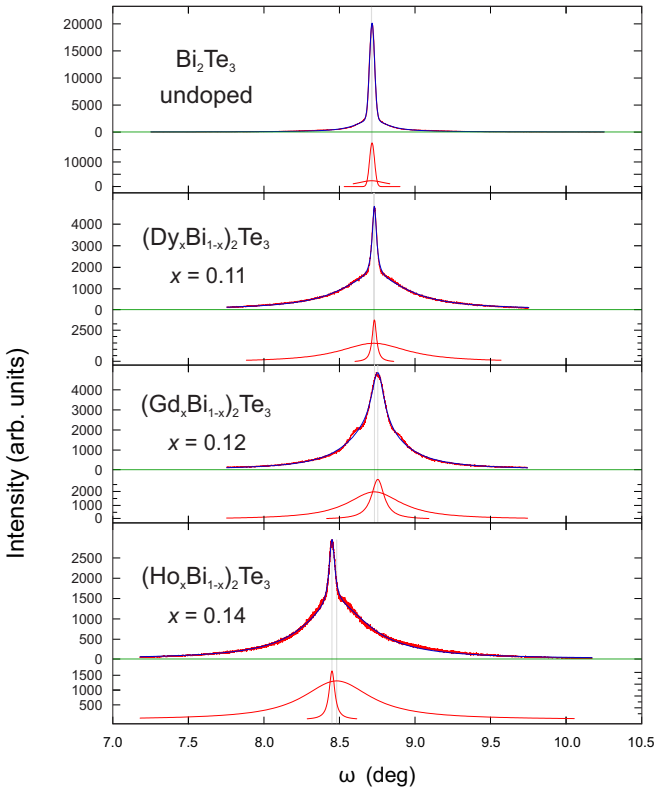

FIG. S2. Rocking curves at the (0 0 6) Bragg reflection for a series of undoped and rare earth doped Bi_2Te_3 thin films. The experimental data (top panels) has been fitted using two Lorentzian peaks (bottom panels), except for the undoped film, where a Lorentzian and a Gaussian peak have been fitted. The fitting parameters are given in Table II. Note that the peak shifts in the doping series are primarily due to different tilt offsets.

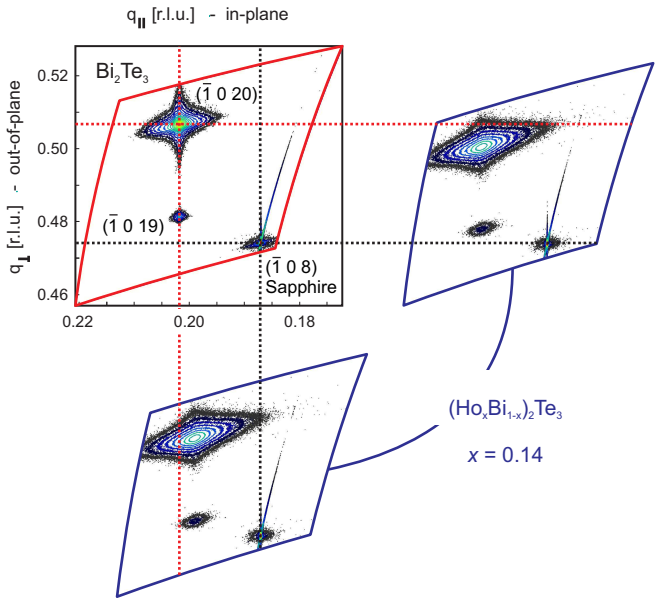

FIG. S3. Reciprocal space mappings obtained for undoped and Ho-doped films with $x = 0.14$. Note the dashed red lines are aligned to the center-most position of the $(\bar{1}\ 0\ 20)$ peak for the undoped sample and the dashed black lines are aligned to the center-most positions of the Al_2O_3 $(\bar{1}\ 0\ 8)$ peaks in each scan.

III. RECIPROCAL SPACE MAPS

XRD asymmetric reciprocal space mappings (RSMs) were obtained using a PANalytical X'Pert PRO diffractometer with Cu Kα_1 emission and a 1D PIXcel detector in grazing-exit configuration. Figure S3 shows RSMs for undoped and Ho-doped ($x = 0.14$) samples. The RSMs were obtained by aligning to the Al_2O_3 $(\bar{1}\ 0\ 8)$ peak and scanning over the relative locations of the Bi_2Te_3 $(\bar{1}\ 0\ 19)$ and $(\bar{1}\ 0\ 20)$ peaks. A misalignment of the substrate and film peaks was observed in these samples which is consistent with our previous Bi_2Te_3 and rare earth doping studies.[2–4] The misalignment in the film and substrate peaks indicates that the thin films grow incoherently on Al_2O_3 with their own in-plane lattice parameters. The in-plane and out-of-plane lattice parameters were calculated from the center positions of the $(Ho_xBi_{1-x})_2Te_3$ $(\bar{1}\ 0\ 20)$ peaks, and are $a = 4.408$ Å and $c = 30.403$ Å for $x = 0$ and $a = 4.402$ Å and $c = 30.579$ Å for $x = 0.14$. An expansion of the out-plane-lattice parameter, determined using the RSM information, is consistent with the trend observed from the peak analysis of the $2\theta-\omega$ scans shown in the main text. The in-plane lattice parameter was found to slightly decrease as a function of Ho

doping concentration. A slight decrease in the a-axis lattice constant is consistent with previous findings on $(Dy_xBi_{1-x})_2Te_3$.[4] Similar to the symmetric XRD scans, the RSMs show peak broadening and an intensity decrease as a function of Ho doping concentration. The peak degradation is particularly evident from the visible reduction in intensity of the weaker $(\bar{1}\ 0\ 19)$ peak for $x = 0.14$ and the complete disappearance of this peak for films grown at higher Ho cell temperatures (not shown).

IV. PHOTON ENERGY DEPENDENT BANDSTRUCTURE

The ARPES measurements were performed at beamline 10.0.1 of the Advanced Light Source (ALS) at Lawrence Berkeley National Laboratory using a Scienta R4000 analyzer. The total convolved energy resolution was 16 meV and and the angular resolution 0.2°, respectively. The sample was prepared by *in-situ* cleaving.[5]

Figure S4 shows ARPES measurements obtained on an *in-situ* cleaved Ho-doped Bi_2Te_3 thin film with $x = 0.14$ as a function of photon energy. No obvious photon energy dependence of the surface state band was observed, despite intensity changes in the spectra, due to matrix element effects. The dispersion of the surface state band and bulk valence band were found to resemble that of undoped Bi_2Te_3.[6] However, the ARPES data for the Ho-doped sample are of lower quality than undoped and Gd- or Dy-doped samples, which is the result of increased scattering-induced broadening of the distribution of the quasiparticle spectral function in energy-momentum space.

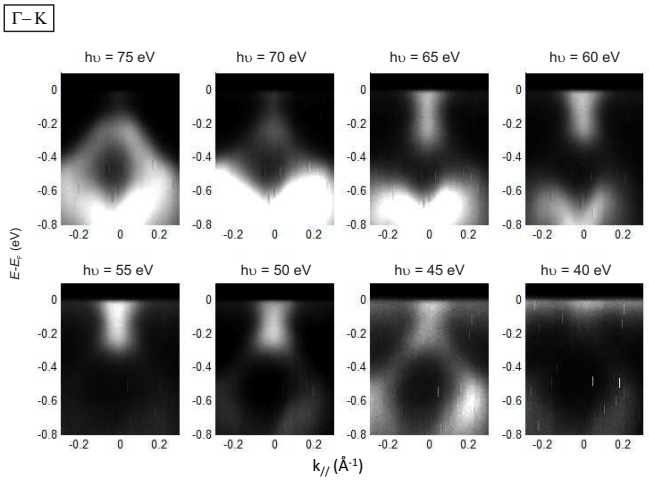

FIG. S4. Band dispersions at different photon energies obtained along the K-Γ-K direction from an *in-situ* cleaved $(Ho_{0.14}Bi_{0.86})_2Te_3$ thin film sample. Both bulk valence band (BVB) and surface state band (SSB) can be resolved. A linear dispersion starting from Dirac point is observed.

V. COMPARISON OF GD-, DY-, AND HO-DOPED BI_2TE_3 THIN FILM SAMPLES

For comparing the structural and magnetic properties of Gd-, Dy-, and Ho-doped Bi_2Te_3 thin films, we have listed all relevant information from Refs. 2–4, 7, and 8 in Tab. V.

TABLE S2. Comparison of the structural and magnetic properties of Gd-, Dy-, and Ho-doped Bi_2Te_3 thin films. x_{RE} is the RE concentration in $(RE_xBi_{1-x})_2Te_3$ and RE the doping concentration in at.-% as determined by Rutherford backscattering spectrometry and particle induced x-ray emission spectroscopy. The c-axis lattice constant has been fitted using a procedure described in Ref. 8. The magnetic moments, given in μ_B per rare earth ion, have been determined by SQUID magnetometry at 5 K for Gd-doped films and at 2 K for Dy- and Ho-doped films.

	x_{RE}	RE at.-%	c (Å)	μ (μ_B/ion)
undoped	-	-	30.39	-
Gd	0.12	4.8	30.62	6.93
	0.16	6.4	30.71	-
	0.27	10.6	30.94	7.00
Dy	0.02	0.9	30.48	13.2
	0.06	2.2	30.51	8.28
	0.11	4.5	30.52	6.26
	0.18	7.3	30.61	4.99
	0.36	14.2	30.79	4.29
Ho	0.14	5.5	30.61	5.20
	0.21	8.4	30.73	5.08

* Corresponding author: Thorsten.Hesjedal@physics.ox.ac.uk

[1] L. J. Collins-McIntyre, N.-J. Steinke, C. J. Kinane, T. R. Charlton, A. Pushp, A. J. Kellock, S. S. P. Parkin, G. van der Laan, S. Langridge, and T. Hesjedal, unpublished (2015).

[2] S. Harrison, S. Li, Y. Huo, B. Zhou, Y.-L. Chen, and J. Harris, Appl. Phys. Lett. **102**, 171906 (2013).

[3] S. E. Harrison, L. J. Collins-McIntyre, S. Li, A. A. Baker, L. R. Shelford, Y. Huo, A. Pushp, S. S. P. Parkin, J. S. Harris, E. Arenholz, G. van der Laan, and T. Hesjedal, J. Appl. Phys. **115**, 023904 (2014).

[4] S. E. Harrison, L. J. Collins-McIntyre, P. Schönherr, A. Vailionis, V. Srot, P. A. van Aken, A. J. Kellock, A. Pushp, S. S. P. Parkin, J. S. Harris, B. Zhou, Y. L. Chen, and T. Hesjedal, Sci. Rep. **5**, 15767 (2015).

[5] S. E. Harrison, B. Zhou, Y. Huo, A. Pushp, A. J. Kellock, S. S. P. Parkin, J. S. Harris, Y. Chen, and T. Hesjedal, Appl. Phys. Lett. **105**, 121608 (2014).

[6] Y.-L. Chen, J. G. Analytis, J. H. Chu, Z. K. Liu, S.-K. Mo, X. L. Qi, H. J. Zhang, D. H. Lu, X. Dai, Z. Fang, S. C. Zhang, I. R. Fisher, Z. Hussain, and Z.-X. Shen, Science **325**, 178 (2009).

[7] S. Li, S. Harrison, Y. Huo, A. Pushp, H. Yuan, B. Zhou, A. Kellock, S. Parkin, Y.-L. Chen, T. Hesjedal, and J. Harris, Appl. Phys. Lett. **102**, 242412 (2013).

[8] S. E. Harrison, L. J. Collins-McIntyre, S.-L. Zhang, A. A. Baker, A. I. Figueroa, A. J. Kellock, A. Pushp, S. S. P. Parkin, J. S. Harris, G. van der Laan, and T. Hesjedal, J. Phys.: Condens. Matter **27**, 245602 (2015).